Macromolecules
ARTICLE

Macromolecules **2010**, *43*, 7793–7799 **7793**
DOI: 10.1021/ma101319j

Rheo-SANS Studies on Shear Thickening in Clay−Poly(ethylene oxide) Mixed Solutions

Makiko Takeda,[†] Takuro Matsunaga,[†] Toshihiko Nishida,[†] Hitoshi Endo,[†] Tsutomu Takahashi,[‡] and Mitsuhiro Shibayama*,[†]

[†]*Institute for Solid State Physics, The University of Tokyo, 5-1-5 Kashiwanoha, Kashiwa, Chiba 277-8581, Japan, and* [‡]*Department of Mechanical Engineering, Nagaoka University of Technology, 1603-1 Kamitomioka, Nagaoka, Niigata 940-2188, Japan*

Received June 16, 2010; Revised Manuscript Received August 6, 2010

ABSTRACT: The structure evolution of network structure in clay−polymer aqueous solutions after shear thickening under shear deformation was investigated by means of small-angle neutron scattering (SANS; Rheo-SANS). Laponite (clay; C) platelet dispersions in poly(ethylene oxide) (PEO; P) aqueous solutions with various deuterious/hydrogeneous water compositions were prepared, and contrast-variation SANS experiments were carried out under flow field. The two-dimensional scattering contour patterns changed suddenly from isotropic to anisotropic patterns at the shear thickening transition point. The orientations of clay platelets and PEO chains were individually characterized by the partial structure factors, $S_{CC}(q)$, $S_{CP}(q)$, and $S_{PP}(q)$, which were obtained by decomposition of the SANS intensity functions. The SANS results show that PEO chains are adsorbed on clay platelets even in a flow field and are peeled off at the shear thickening transition point. Flow birefringence results suggest that the shear thickening is a corporation of clay and polymer chains, i.e., bridging of clays by PEO chains. Aging of the clay−PEO solutions leads to lowering the threshold of the critical shear rate at which shear thickening occurs.

Introduction

It is known that polymer stabilizes colloidal suspension, and these particle−polymer complexes have a sense of future potential in industrial application, e.g., personal care products, food, and so on.[1−4] Another reason for adding polymers to colloidal suspension is to achieve desired rheological properties, in which polymers are used to control the viscosity. Addition of polymers gives rise to many novel properties, such as shear thinning, shear thickening, gelation, etc.[5] It is known that shear thinning occurs with structural destruction or orientation, while shear thickening is accompanied by structure formation. Generally, the polymer chains are partially adsorbed on the colloidal particles. By shearing, polymer chains are aligned and stretched along the flow direction, resulting in bridging neighboring particles. As a result, shear thickening occurs.[6] Inorganic clay, Laponite, disk-shaped platelets in nanometer order, also forms a colloidal suspension in water. Because the clay platelets have negative charges on the surface and positive charges on the edge, the platelets themselves are capable of gel formation with the so-called "card-house" structure.[7] Interactions between clay particles depend highly on the solution properties such as pH and ionic strength as well as clay concentration.[8,9] It is also reported that rheology of clay suspension changes with time, i.e., aging effect.[10−15]

Nanocomposite polymer hydrogels have been gathering much attention in recent years. For example, Schexnailder and Schmidt reviewed recent advancement of hydrogels and their biotechnological applications.[16] Among a variety of studies on nanocomposite gels, clay−poly(ethylene oxide) (PEO) mixtures are known to have interesting features, such as adsorption of PEO polymer chain on clay platelets,[17−20] aging characteristics,[17,21,22] and presence of a limited clay−PEO concentration region where shear thickening takes place.[23,24] Here, the interparticle distance and the sizes of polymer chains and the particle play a major role in shear thickening.[25] Since the sizes of clay particles and PEO chains are in nanometer order and the neutron scattering length densities of clay and PEO are between H_2O and D_2O, small-angle neutron scattering (SANS) is one of the most suitable means for structural investigation of clay−PEO mixtures in water. So far, it has been reported by SANS that both clay platelets and polymer chains oriented under shear field,[26] leading to shear thinning.[27,28] Recently, we carried out Rheo-SANS experiments on shear thinning of clay−PEO aqueous solutions,[29] where we employed contrast variation SANS (CV-SANS) and decomposition method[30] to extract the information on clay−polymer interaction. In this paper, we report structural analysis of shear thickening of clay−PEO mixtures with CV-Rheo-SANS as well as aging effects of the clay−PEO mixtures in water elucidated by rheological and dynamic light scattering (DLS) measurements.

Experimental Section

Samples. A synthetic clay, Laponite-XLG, with radius $R_C \sim 150$ Å and thickness $D_C \sim 10$ Å was obtained from Rockwood Additives Limited, U.K. The empirical formula is given by $[Mg_{5.34}Li_{0.66}Si_8O_{20}(OH)_4]Na_{0.66}$. The laponite clays are 2:1 phyllosilicates, meaning that two tetrahedral layers of atoms are sandwiching an octahedral layer of atoms. Poly(ethylene oxide) (PEO) with the viscosity-average molecular weight $M_v = 400 \times 10^3$ g/mol was purchased from Sigma-Aldrich Co. The hydrodynamic radius, R_h, and the radius of gyration, R_g, in water were evaluated to be 660 and 400 Å, respectively.[31] Hence, the chain overlap concentration is estimated to be 0.0025 g/cm^3. The solvent deuterium oxide (D_2O) was purchased from Cambridge Isotope Laboratories, Inc. (CAS 7789-20-0), and the hydrogenated water (H_2O) was obtained from a Milli-Q Element.

*To whom correspondence should be addressed: e-mail shibayama@issp.u-tokyo.ac.jp; Ph +81-4-7136-3418; Fax +81-4-7134-6069.

Published on Web 08/16/2010

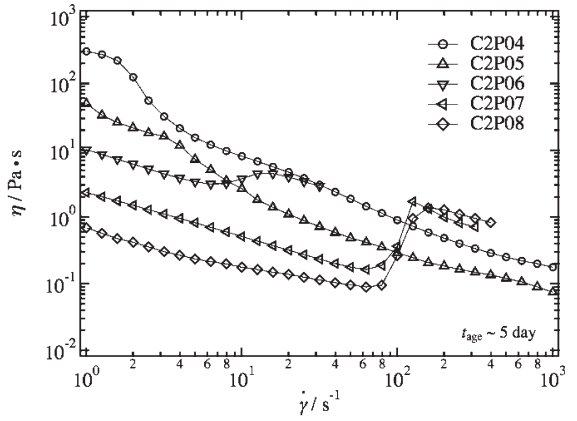

Figure 1. Viscosity behavior of clay−PEO aqueous solutions at various PEO concentrations as a function of shear rate. Clay concentration was fixed to 2 wt %. There is a small concentration window in which shear thickening is observed.

Samples were prepared by simply mixing the clay and PEO powders into mixtures of H_2O/D_2O, followed by vigorous stirring for 24 h at room temperature. The sample code was defined in such a way that C2P04 indicates clay 2 wt % and PEO 0.4 wt % solution. The solvent composition was varied depending on the experiments, e.g., 100% H_2O for flow birefringence. D_2O was used as a solvent for most experiments not only for SANS (ϕ_{D_2O} = 1.0, 0.9, 0.8, 0.7, 0.0) but also for rheological measurements (ϕ_{D_2O} = 1.0, 0.0). All measurements were performed at room temperature, T = 25 °C.

Rheological Measurement. Rheological measurements were carried out on an MCR-501 (Anton Paar, Physica, Austria) with cone−plate geometry. The radius of the plate was 25.0 mm, and the cone angle was 0.99°.

Rheo-SANS. Small-angle neutron scattering experiments were carried out at two-dimensional SANS instrument, SANS-U, Institute for Solid State Physics, The University of Tokyo.[32] The wavelength of incident neutrons was λ = 7.0 Å (±10%), and the sample-to-detector distances (SDD) were 2, 4, and 8 m. This setup allowed us to obtain SANS intensity functions, $I(q)$, in the range of $0.005 \le q \le 0.2$ Å^{-1}. Here, q is the magnitude of the scattering vector, i.e., $q \equiv (4\pi/\lambda) \sin\theta$, where 2θ is the scattering angle. Rheo-SANS experiments were carried out with MCR-501 on SANS-U. A double-cylinder-type shear cell made of quartz was used. The diameters of the outer and the inner cylinders were 50.0 and 48.0 mm, respectively, and the gap was 1.00 mm. Two-dimensional (2D) SANS intensity profiles (SDD = 2, 4, and 8 m) in the radial direction were obtained under a shear flow. A series of samples with different scattering length densities of solvent were prepared. The scattering length densities were calculated on the basis of their chemical structures and mass densities. The densities of clay and PEO are 2.65 and 1.13 g/cm^3, respectively. The CV-SANS measurement was carried out with several D_2O fractions (ϕ_{D_2O} = 1.0, 0.9, 0.8, 0.7, 0).

DLS. Dynamic light scattering experiments were carried out with an ALV5000 SLS/DLS apparatus, ALV, Germany, at a fixed scattering angle of 90°. The light source was a 22 mW He−Ne laser (wavelength λ = 632.8 nm).

Rheo-BF. Birefringence measurement under the flow (Rheo-BF) was carried out with MCR-501 on the Optical Analyzer Module 2ch version (OAM 2ch).[33,34] A parallel-plate type shear cell made of quartz was used for Rheo-BF. The radius of the cell was 21.4 mm, and sample thickness was 1.00 mm.

Results and Discussion

Shear Thickening and Aging Effects in Clay−Polymer Mixtures in an Aqueous Solution. Figure 1 shows the shear rate, $\dot{\gamma}$, dependence of the viscosity, η, of clay−PEO aqueous solutions (C2Py) with various PEO concentrations, where the clay concentration was fixed to be 2 wt %. The measurements were carried out 5 days after sample preparation as will be shown in Figure 5. This figure indicates various interesting features of the clay−PEO aqueous solutions. (1) The viscosity decreases by increasing PEO concentrations, and in most cases shear thinning occurs with $\dot{\gamma}$. (2) Only C2P07 and C2P08 show a shear thickening behavior at critical shear rate ($\dot{\gamma}_{cri} \sim 10^2$ s^{-1}). This indicates that shear thickening strongly depends on the concentrations of both solutes, i.e., clay and PEO. The lowering of the zero shear viscosity with PEO concentration is very intriguing. As will be discussed later, this phenomenon is ascribed to (i) viscosity increase of clay solution by aging and (ii) a delicate balance among the volume fractions of clay and polymer and the interclay distance. A clay solution itself becomes viscous as a result of aging. When a small amount of PEO is added to a 2 wt % clay solution ($C_{PEO} \approx 0.4$ wt %, $t_{age} \sim 5$ day), this addition does not interfere with formation card-house structure, while temporally bridging clay platelets by PEO chains, resulting in viscosity increase. Further addition of PEO ($0.4 \le C_{PEO} \le 0.8$ wt %, $t_{age} \sim 5$ day) leads to screening of clay−clay interaction, but wrapping clay platelets. This leads to a dramatic suppression of viscosity as shown in Figure 1. Further addition of PEO ($C_{PEO} \gg 0.8$ wt %) recovers a bridging and viscosity increases. The power law index in the low shear rate region was obtained as follows: 0.87 (C2P06), 0.64 (C2P07), and 0.84 (C2P08). Shear thickening sample shows shear thinning behavior at low shear rate ($\dot{\gamma} < \dot{\gamma}_{cri}$). This is attributed to peeling off of PEO chains from clay surfaces by shearing. Because the absorption spots on clay surface appear with desorption of PEO, adsorption goes along with peeling off at low shear rate.

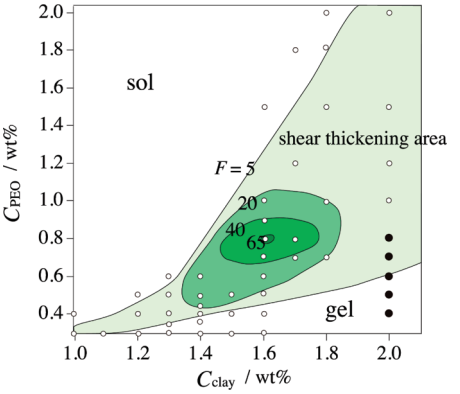

Figure 2. Shear thickening contour map as a function of PEO and clay concentrations. The degree of shear thickening, F, after 1 day aging (i.e., $t_{age} \sim$ 24 h) is plotted as a function of PEO and clay concentrations.

In order to grasp the concentration window where shear thickening occurs, we constructed a shear thickening map. Figure 2 shows the contour map of the shear thickening factor at 25 °C as a function of clay and PEO concentrations. Here, the shear thickening factor was defined by the viscosity ratio at $\dot{\gamma}_{cri}$ before ($\dot{\gamma} \to \dot{\gamma}_{cri} + 0$) and after shear-thickening transition ($\dot{\gamma} \to \dot{\gamma}_{cri} - 0$)

$$F \equiv \frac{\eta_{aft}}{\eta_{bef}} \tag{1}$$

As shown in the map, the concentration region where a strong shear thickening occurred was limited in a small concentration window, i.e., $1.4 \le C_{clay}$ (wt %) ≤ 1.9 wt % and

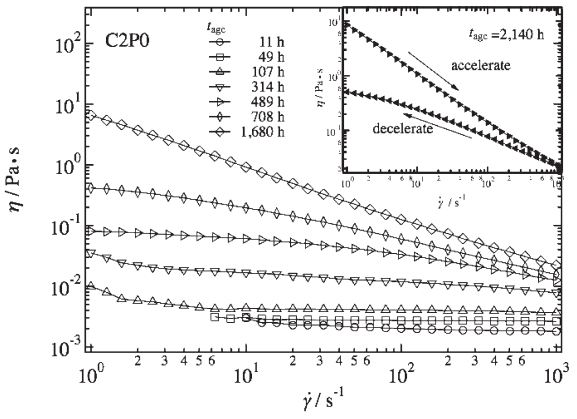

Figure 3. Viscosity vs shear rate curves of clay 2 wt % aqueous solution (C2P0) changing with time. Inset is hysteresis curve of C2P0 at t_{age} = 2140 h. As shown, C2P0 follows different curves between accelerate and decelerate.

$1.2 \leq C_{PEO}$ (wt %) ≤ 2.2 wt % for $F > 20$. Similar diagrams were obtained in silica−polymer mixture solutions[23,24,35] and nanoemulsion−polymer mixture solutions.[36] Although it was preferable to study this region, the shear thickening effect was too strong to be investigated by a rheometer, and samples were spun off from the chamber. Hence, we chose the region at C_{clay} = 2.0 wt % (shown by filled circles) for further investigation of the shear thickening phenomena.

Note that contrary to the case studied here, clay−PEO solutions with C_{clay} = 3 wt %, C_{PEO} = 2 wt %, and the molecular weight of 1000 kg/mol exhibit a shear thinning behavior.[29] This is due to the fact the clay platelets are wrapped by PEO chains and the clay platelets lose their strong interaction, resulting in domination of the viscoelastic properties of polymer solutions.

Aging Effects of Clay Dispersions. It is well-known that clay dispersions in aqueous solutions undergoes significant shear thickening followed by gelation.[37,38] Hence, it is of particularly importance to clarify the aging effect of clay dispersion before exploring clay−polymer mixture solutions. Figure 3 shows time evolution of the shear viscosity, η, of clay dispersion C2P0 (C_{clay} = 2 wt %) in water (ϕ_{D_2O} = 0). As shown in the figure, the viscosity, η, increased with aging time, t_{age}. The sample was vigorously stirred for 24 h after mixing clay powder in water. The aged data at t_{age} = 11 h were taken by sampling a portion of the sample at t_{age} = 11 h before completion of stirring. As shown in the figure, the viscosity increased with time and shear thinning occurred by shearing. Mourchid et al.[38] reported that this type of viscosity increase is ascribed to ionic strength changing with time. That is, an increase in Mg^{2+} induced by dissolution of carbon dioxide into solution caused gelation. The inset shows the hysteresis loop of C2P0 aged for t_{age} = 2140 h in the η vs $\dot{\gamma}$ plot, indicating that the card-house structure is significantly destroyed by shearing.

In order to elucidate the time evolution of the structure of clays in a solution, we carried out a DLS measurement. Figure 4a shows time evolution of DLS correlation functions, $g^{(2)}(\tau)$, of clay dispersion C2P0 (C_{clay} = 2 wt %) in water (ϕ_{D_2O} = 0), where τ is the decay time. Figure 4b shows the cluster distribution function, $G(\Gamma)$, as a function of the characteristic decay time, Γ^{-1} ($=\tau$). $G(\Gamma)$ was obtained by taking inverse Laplace transform of $g^{(2)}(\tau)$ via the CONTIN program.[39] As shown in the figure, the distribution function is bimodal at t_{age} = 11 h. The hydrodynamic radii, R_h, of the clay platelets are 400 Å and 2.0×10^3 Å and are assigned to the fast and slow modes, respectively. By aging, the correlation

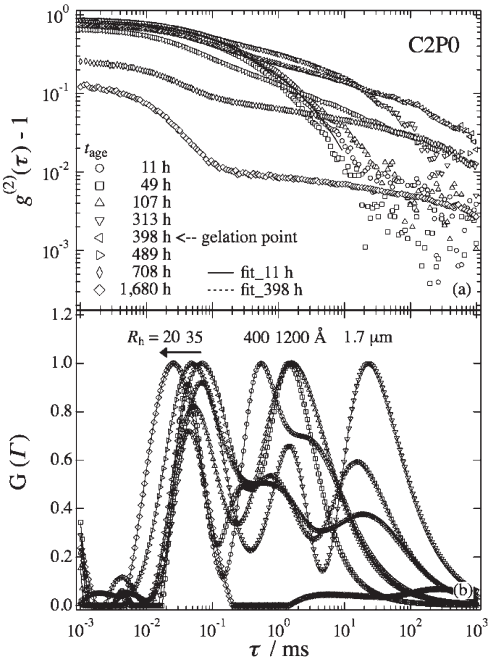

Figure 4. (a) Time evolution of DLS correlation functions, $g^{(2)}(\tau)$, of clay dispersion C2P0. As shown, gelation point is t_{age} = 313 h. (b) The cluster size distribution function, G(Γ).

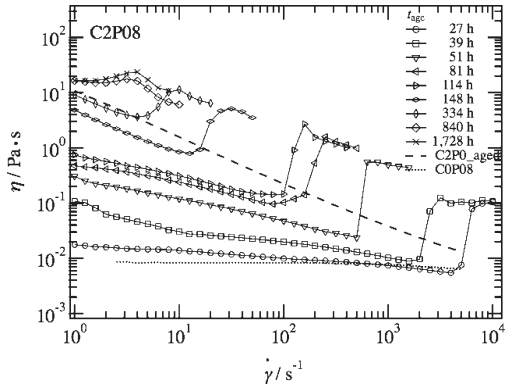

Figure 5. Rheology of C2P08 changing with time. Vertical axis is viscosity η, and horizontal axis is shear rate $\dot{\gamma}$. The larger the aging time, the smaller is the critical shear rate at which shear thickening takes place.

function becomes broader with tailing, and the peak in $G(\Gamma)$ moves to $\Gamma^{-1} \approx 20$ ms ($R_h \approx 1.7$ μm) up to t_{age} = 398 h. Above this t_{age}, the initial amplitude decreases and a faster relaxation appears around $R_h \approx 20-35$ Å. According to the previous studies on gelation process by DLS, this process means gelation and postgelation with the gel point at t_{age} = 398 h.[40] As demonstrated here, one must bear in mind the presence of aging effects in investigation of the structure−rheological property relationship of clay-containing materials.

Aging Effects of Clay−Polymer Mixture Solutions. Figure 5 shows time evolution of the shear viscosity for clay−dispersed polymer solution, C2P08 (C_{clay} = 2 wt %), in water. The dotted line in the bottom shows the viscosity data of C0P08 (i.e., 0.8 wt % PEO solution), which does not show any shear rate dependence. As shown in the figure, on the other hand, the viscosity of C2P08 increased from that of polymer solution (ca. 10^{-2} Pa·s) to 20 Pa·s by aging for t_{age} = 1728 h. The viscosity of the PEO−clay mixture at $\dot{\gamma}$ = 1 s^{-1} and t_{age} = 1728 h is about 5 times larger than that of clay aqueous dispersion (C2P0) at t_{age} = 1680 h (see Figure 3). This increase is due to aging and changing ionic strength.[22,38] Another interesting feature is the

following. At the beginning of aging, the viscosity is rather low and showed a shear thinning up to $\dot{\gamma} \approx 4000\ s^{-1}$. However, the critical shear rate $\dot{\gamma}$ ($= \dot{\gamma}_{cri}$) at which shear thickening took place becomes smaller by aging. Concurrently, the viscosity at low shear rate (e.g., $\dot{\gamma} = 1\ s^{-1}$) increased as well. This indicates that aging affects the shear thickening and promotes it.

The onset of sol−gel transition can be precisely monitored by dynamic light scattering.[41] Figure 6 shows the time evolution of DLS correlation function of C2P08 during aging.

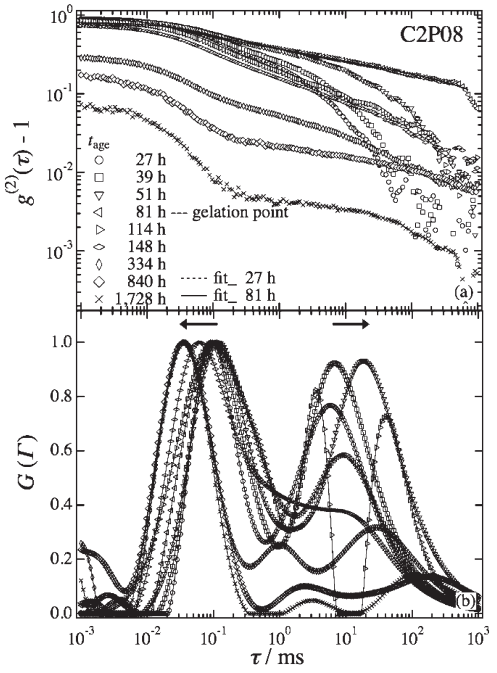

Figure 6. (a) Time evolution of DLS correlation functions for C2P08 as a function of aging time. Here, $t_{age} = 81$ h is gelation point. Correlation functions of $t_{age} < 81$ h can be fitted by eq 2, while that of $t_{age} \geq 81$ h was eq 3. (b) The cluster size distribution function, G(Γ).

Table 1. Fitting Parameters of $g^{(2)}(\tau) - 1$

	time (h)	S_I	D ($\times 10^{-8}$)/ cm^2 s^{-1}	A	$t_c t^*$/ ms	t_{max}/ ms	b	D_p
C2P08	27	0.98	27	0.23	6.0		0.39	
	81	0.90	33	0.088	0.021	8000		0.85
C2P0	11	0.96	16	0.13	2.1		0.41	
	398	0.86	50	0.082	0.018	2700		0.76

In a sol state, the correlation functions can be fitted with a combination of single- and stretched-exponential functions. As a matter of fact, the DLS data could be fitted with the following function for $t_{age} < 81$ h.

$$g^{(2)}(\tau) - 1 = \sigma_I^2\{A \exp(-Dq^2\tau) + (1-A)\exp[-(\tau/\tau_c)^{\beta}]\}^2 \quad (2)$$

where σ_I^2 is the initial amplitude of the scattering intensity−time correlation function $g^{(2)}(\tau)$. A is the fraction of the fast mode, D is the collective diffusion coefficient, τ_c is the characteristic decay time for the slow mode, and β is the stretched exponent. At the sol−gel transition threshold, the correlation function becomes a power-law function

$$g^{(2)}(\tau) - 1 = \sigma_I^2\left\{A \exp(-Dq^2\tau) + \frac{(1-A)\exp-(\tau/\tau_{max})}{[1+(\tau/\tau^*)]^{(1-D_p)/2}}\right\}^2 \propto \tau^{-(1-D_p)} \quad (3)$$

where τ^* is the characteristic time where the power-law behavior appears. Note that an exponential term with the large τ cutoff τ_{max} is added in eq 2. D_p is the fractal dimension of $g^{(2)}(\tau)$. As shown in the figure, the sol−gel transition occurred at $t_{age} \approx 81$ h. For $t_{age} \geq 81$ h, nonergodicity appeared, resulting in a lowering of the intercept of $g^{(2)}(\tau)$. The fitting parameter is shown in Table 1 together with those for C2P0 at $t_{age} = 11$ h (sol state) and at $t_{age} = 398$ h (sol−gel transition point). By comparing these two data sets, it can be deduced that the addition of PEO to clay aqueous dispersion results in accelerating of gelation. This is due to the fact that shear-induced polymer stretching accelerates a percolation process by bridging neighboring platelets with polymer chains.

SANS of C2P08 at the Shear Thickening Point. Let us discuss the structure change of C2P08 after shear thickening. Figure 7 shows the viscosity and SANS pattern changes of C2P08 at $t_{age} \approx 51$ h (of Figure 5) as a function of $\dot{\gamma}$. Constant shear rates were applied to C2P08 for roughly 100 s each, followed by stepwise changes in $\dot{\gamma}$. For $\dot{\gamma} \leq 400\ s^{-1}$, no significant changes were observed in both the viscosity and SANS patterns, but a slight shear thinning. On the other hand, a drastic increase in η by a factor of 100 was observed at $\dot{\gamma} = 500\ s^{-1}$. Concurrently, the SANS pattern changed to an anisotropic pattern with its long axis perpendicular to the flow direction.

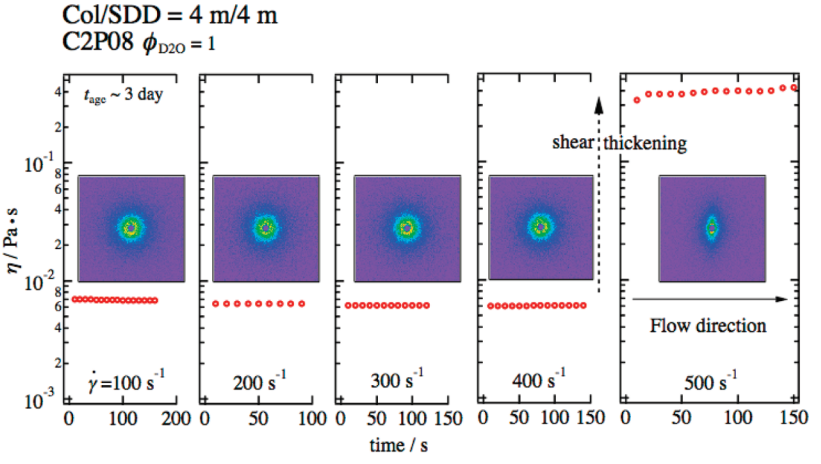

Figure 7. SANS patterns for C2P08 at various shear rates. A drastic jump in viscosity occurs between $400 < \dot{\gamma} < 500\ s^{-1}$ occurs. After shear thickening, the SANS pattern changed to anisotropic having a long axis perpendicular to the flow direction.

Figure 8 shows two-dimensional SANS patterns for C2P08 in pure D_2O (i.e., $\phi_{D_2O} = 1.0$) at various shear rates, $\dot{\gamma}$. The figures in the upper and lower columns are those obtained with the sample-to-detector distance (SDD) = 2 and 8 m, respectively.

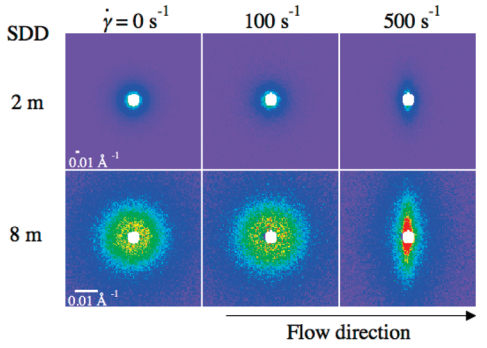

Figure 8. SANS patterns for clay−PEO solutions (C2P08) undergoing shear thickening. Shear thinning and shear thickening occur at 100 and 500 s^{-1}, respectively. The sample-to-detector distances (SDD) were 2 m (top) and 8 m (down).

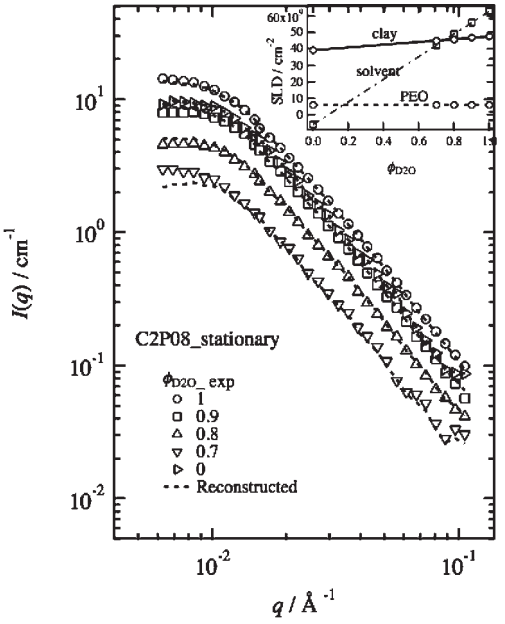

Figure 9. Scattering intensities of C2P08 at several solvent compositions in a stationary state ($\phi_{D_2O} = 1.0, 0.9, 0.8, 0.7, 0.0$).

As shown here, anisotropic patterns appeared when $\dot{\gamma} = 500$ s^{-1}. Hence, it is deduced that the shear thickening is strongly correlated with a structure change in nanoscopic order. Note that the value of $\dot{\gamma}_{cri}$ was higher in Figure 7 rather than in Figure 1. This is due to an aging effect and the history of shearing as discussed in Figures 3 and 4.

Contrast-Variation Rheo-SANS and Rheo-BF. Figure 9 shows circularly averaged SANS scattering intensity functions, $I(q)$s, of C2P08 at various solvents differing in the D_2O/H_2O ratio (i.e., $\phi_{D_2O} = 1.0, 0.9, 0.8, 0.7, 0.0$). These $I(q)$s were decomposed to three partial structure factors, i.e., $S_{CC}(q)$, $S_{CP}(q)$, and $S_{PP}(q)$, by use of the following equation:[42,43]

$$I(q) \approx \Delta\rho_C{}^2 S_{CC}(q) + 2\Delta\rho_C\Delta\rho_P S_{CP}(q) + \Delta\rho_P{}^2 S_{PP}(q) \quad (4)$$

Here, $\Delta\rho_C$ and $\Delta\rho_P$ are the differences of scattering length densities of clay and solvent and that of PEO. In a similar way, $I(q)$s for C2P04, C2P05, C2P06, C2P07, and C2P08 were also decomposed. The decomposition was carried out by using the method developed by Endo et al.[44] Figure 10 shows the decomposed partial-structure factors (a) $S_{CC}(q)$, (b) $S_{CP}(q)$, and (c) $S_{PP}(q)$ for C2Py (y = 04−08). Note that $S_{CC}(q)$ does not seem to be a function of C_{PEO}. This indicates the clay structure; e.g., the interclay distance and the orientation are not affected by addition of PEO. On the other hand, $S_{PP}(q)$ shows a clear C_{PEO} dependence. The larger C_{PEO}, the larger the $S_{PP}(q)$ is. This result is reasonable because the scattering intensity increases with the concentration for the case that the solution is in the dilute regime. However, the shape of $S_{PP}(q)$ changes by increasing C_{PEO}, and $S_{PP}(q)$ started to have a peak around $q = 8 \times 10^{-3}$ Å^{-1}. In the case of polymer solutions, such a scattering maximum was not observed even in the presence of interpolymer interaction. We conjecture that this is due to an interference of the polymer chains adsorbed on clay platelets. This issue will be discussed later in more detail.

The solid lines in Figure 10 were obtained by curve fitting. Fitting functions are given by Matsunaga et al.[45] Table 2 shows these fitting parameters. The parameters, the radius of clay R_C and the thickness of clay D_C, were fixed to be the same as those for clay dispersion. The clay volume fraction ϕ_{cyl} is given by stoichiometry. The Percus−Yevick radius for nanocomposite gels[46] R_{PY} was obtained by curve fitting, which was an increasing function with increasing polymer concentration. From S_{PP}, the correlation length ξ was evaluated to be around 100 Å. From S_{CP}, one can learn about

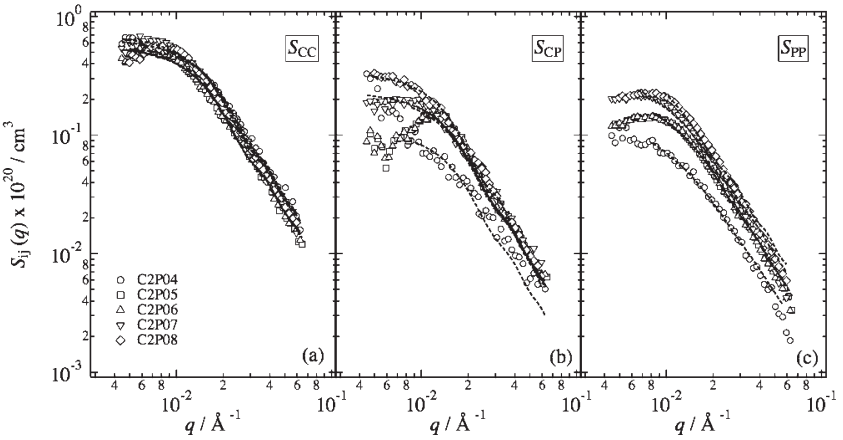

Figure 10. Decomposed CV-SANS patterns, $S_{CC}(q)$, $S_{CP}(q)$, and $S_{PP}(q)$, for stationary measurements. Concentration is C2P04, C2P05, C2P06, C2P07, and C2P08.

the structure near the clay surface. First of all, there exists a polymer-adsorbed layer. The radius of the layer is an increasing function of polymer concentration, while the thickness of the layer, i.e., $D_{pl} - D_C$, is rather independent. The polymer fraction in the adsorbed layer is much higher than that of medium.

Figure 11 shows scattering intensity of C2P08 at $\dot{\gamma} = 500\ s^{-1}$. As is shown in Figure 8, anisotropic patterns were observed in $I(q)$s exclusively at $\dot{\gamma} = 500\ s^{-1}$. We took sector averages of these scattering patterns. Here, sector average with the sector angle of $\pm 20°$ was taken along parallel (para) and perpendicular (perp) to the flow direction.

Figure 12 shows the comparison of the decomposed scattering intensity functions, i.e., $S_{CC}(q)$, $S_{CP}(q)$, and $S_{PP}(q)$ at $\dot{\gamma} = 0$, 100, and 500 s^{-1}. For $\dot{\gamma} = 0$ and 100 s^{-1}, no anisotropy was found in any of the partial structure factors, $S_{CC}(q)$, $S_{CP}(q)$, and $S_{PP}(q)$. At $\dot{\gamma} = 500\ s^{-1}$, on the other hand, the partial structure factors in the parallel (para) direction differs significantly from that in the perpendicular (perp) direction. In both $S_{CC}(q)$ and $S_{PP}(q)$, the intensity in the perpendicular direction is larger than the parallel direction, i.e., $S_{ii\_perp}(q) \gg S_{ii\_para}(q)$. These are due to parallel orientations of both clay platelets and polymer chains. On the other hand, both components of $S_{CP}(q)$ decreases by shear thickening. This indicates peeling-off of polymer chains occurs on the clay surface. SANS data sets, which show isotropic scattering pattern (Figures 7 and 8), indicate dominance of peeling-off under low shear field. When increasing of shear rate, many absorption spots are bared by peeling-off from clay surfaces and PEO chains can cross-link between neighboring clays. Like this, shear thickening takes place.

Figure 13 shows shear rate dependence of (a) the viscosity, η, and (b) the flow birefringence (Rheo-BF), Δn, after loading stepwise shear rates starting from 0 to 1, 5, 30, 1, and 0 s^{-1}. Though the viscosity for C0P08 does not depend

Table 2. Stationary Fitting Parameters

	C2P04	C2PO5	C2FO6	C2P07	C2P08
R_c/Å			150		
D_C/Å			10		
ϕ_{cyl}			0.0076		
R_{PY}/Å	91	72	76	76	110
prefactor	1.6	1.2	1.2	1.5	1.6
R_{Pl}/Å	150	150	150	150	190
D_{Pl}/Å	17	21	21	21	14
ϕ_{pl}	0.23	0.39	0.38	0.30	0.21
S^0_{PP}	0.082	0.12	0.14	0.19	0.25
ξ/Å	110	120	120	130	180

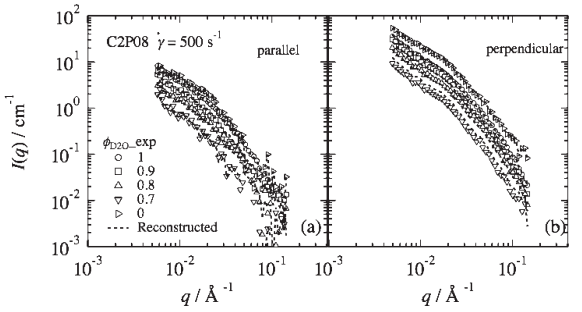

Figure 11. Sector-averaged $I(q)$s of C2P08 at $\dot{\gamma} = 500\ s^{-1}$ which show anisotropic patterns. Sector average with the sector angle of $\pm 20°$ was taken along (a) parallel and (b) perpendicular to the flow direction.

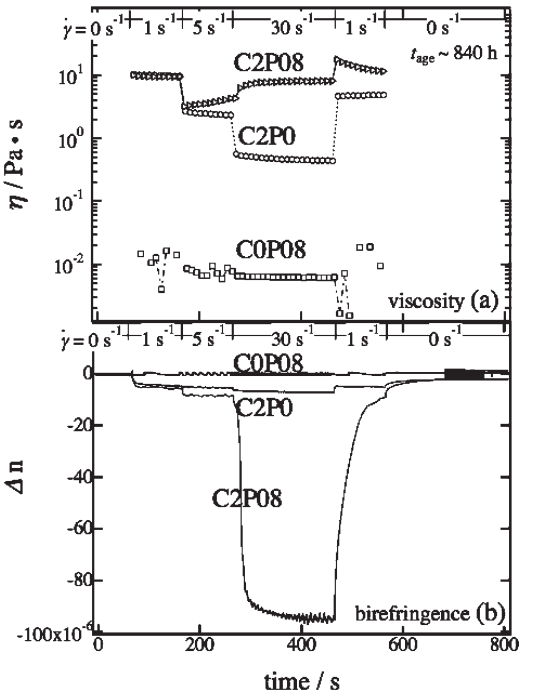

Figure 13. Shear-rate dependence of (1) viscosity, η, and (2) the birefringence, Δn, after loading stepwise shear rates. Δn of C2P08 changes suddenly by loading $\dot{\gamma} = 30\ s^{-1}$, followed by vigorous oscillation. After reducing $\dot{\gamma}$ to 1 s^{-1}, Δn is reduced to 0 (offset value). The viscosity behavior was well correlated to Δn. There were little Δn changes in the clay and PEO solution.

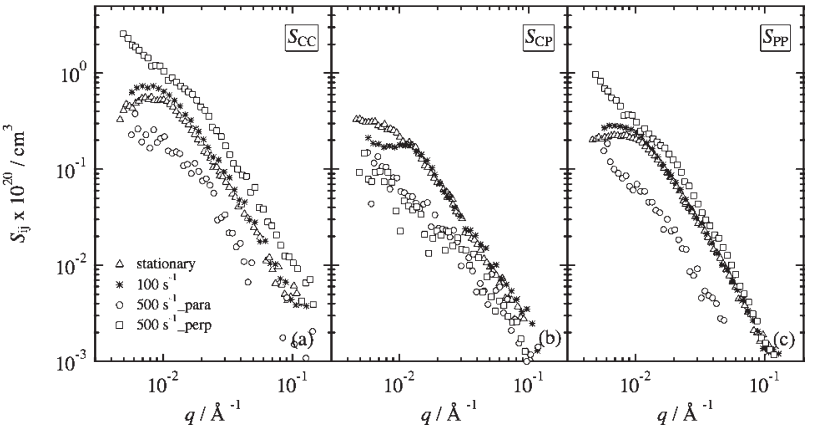

Figure 12. Sector-averaged CV-SANS patterns after decomposition, $S_{CC}(q)$, $S_{CP}(q)$, and $S_{PP}(q)$: open triangles (0 s^{-1}), cross symbol (100 s^{-1}), open circles (500 s^{-1}, parallel), and open squares (500 s^{-1}, perpendicular).

on the shear rate, that of C2P0 shows shear thinning. On the other hand, the mixture C2P08 shows shear thickening when a stepwise change in $\dot{\gamma}$ was applied from 5 to 30 s^{-1}. Simultaneously to the viscosity, Δn changes suddenly to a large negative value by loading $\dot{\gamma} = 30\ s^{-1}$. The negative oscillation comes from molecular orientation in gel. This suggests that by applying a shear rate of $\dot{\gamma} = 30\ s^{-1}$, elongated PEO chains bridges the clay platelets, resulting in percolation transition. As a result, the clay platelets orient parallel to the flow direction and show negative birefringence and shear thickening due to shear-induced sol−gel transition. After reducing $\dot{\gamma}$ from 30 to 1 s^{-1}, Δn is reduced to 0 (offset value), while a further shear thickening was observed. This indicates that the percolated network remains for a while even after reducing shear flow, resulting in a further increase in η. On the other hand, the reduction of the shear flow decreases in the optical anisotropy. Hence, as explained above, the viscosity behavior was well correlated to Δn. More quantitative investigations, particularly in evaluation of the birefringence as a function of the shear rate, are in progress.

Conclusion

Shear thickening behaviors in clay−PEO aqueous solutions were investigated by Rheo-SANS as a function of clay and PEO concentrations. Rheological and DLS measurements revealed the following. Though both clay dispersions and clay−PEO mixtures showed aging effects, only clay−PEO mixtures underwent shear thickening. It was also elucidated from rheological measurements that the larger the aging time, the smaller is the critical shear rate at which shear thickening takes place. The shear thickening itself is due to bridging of clay platelets with PEO chains. Concurrently, the aging effect and the thickening behavior were investigated by DLS. It was found that the aging contributes both to an increase of relaxation time (from τ_c to τ^* and τ_{max}) and to the thickening behavior.

We employed contrast variation Rheo-SANS (CV-Rheo-SANS) measurement on structural analysis of shear thickening. It was revealed from CV-SANS for nonsheared samples that significant amount of PEO chains are adsorbed on clay platelets. CV-Rheo-SANS data showed that both clay platelets and PEO chains keep random orientation below the shear thickening threshold but orient jumpwise at the threshold by orienting the clay plane parallel to the flow direction. At the same time, PEO chains adsorbed on clay platelets were peeled off and participated in bridging neighboring clay platelets. A parallel orientation of PEO chains to the flow direction was confirmed by Rheo-BF. The shear thickening is reversible. When the shear rate is increased, a shear thickening occurs as a result of bridging. On the other hand, by reducing the shear rate, PEO chain contraction is stronger than shear flow, leading to a decrease in the viscosity. Hence, the shear thickening is a dynamic equilibrium between bridging by chain stretching and contraction controlled by the shear rate.

References and Notes

(1) Napper, D. H. *Polymeric Stabilization of Colloidal Dispersions*, Academic Press: London,1984.
(2) El-Aasser, M. S.; Fitch, R. M. *Future Directions in Polymer Colloids*, Martinus Nijhoff: Dordrecht, 1987.
(3) Parker, A.; Gunning, P. A.; K., N.; Robins, M. M. *Food Hydrocolloids* **1995**, *9*, 333–342.
(4) Nasu, A.; Otsubo, Y. *J. Colloid Interface Sci.* **2006**, *296*, 558–564.
(5) Otsubo, Y. *Nihon Reoroji Gakkaishi* **2003**, *31*, 15–22.
(6) Kamibayashi, M.; Ogura, H.; Otsubo, Y. *J. Colloid Interface Sci.* **2008**, *321*, 294–301.
(7) van Olphen, H. *Clay Colloid Chemistry*, 2nd ed.; John Wiley: New York, 1977.
(8) Li, L.; Harnau, L.; Rosenfeldt, S.; Ballauff, M. *Phys. Rev. E* **2005**, *72*, 051504.
(9) Pignon, F.; Magnin, A.; Piau, J.-M.; Cabane, B.; Lindner, P.; Diat, O. *Phys. Rev. E* **1997**, *56*, 3281–3289.
(10) Kroon, M.; Wegdam, G. H.; Sprik, R. *Phys. Rev. E* **1996**, *54*, 6541.
(11) Bonn, D.; Tanaka, H.; Wegdam, G.; Kellay, H.; Meunier, J. *Europhys. Lett.* **1998**, *45*, 52–57.
(12) Bonn, D.; Tanase, S.; Abou, B.; Tanaka, H.; Meunier, J. *Phys. Rev. Lett.* **2002**, *89*, 015701.
(13) Knaebel, A.; Bellour, M.; Munch, J. P.; Viasnoff, V.; Lequeux, F.; Harden, J. L. *Europhys. Lett.* **2000**, *52* (1), 73–79.
(14) Abou, B.; Bonn, D.; Meunier, J. *Phys. Rev. E* **2001**, *64* (2), 27–41.
(15) Ruzicka, B.; Zulian, L.; Ruocco, G. *J. Phys.: Condens. Matter* **2004**, *16* (42), S4993–S5002.
(16) Schexnailder, P.; Schmidt, G. *Colloid Polym. Sci.* **2009**, *287*, 1–11.
(17) Nelson, A.; Cosgrove, T. *Langmuir* **2004**, *20* (6), 2298–2304.
(18) Lal, J.; Auvray, L. *J. Appl. Crystallogr.* **2000**, *33*, 673–676.
(19) Lal, J.; Auvray, L. *Mol. Cyrst. Liq. Cryst.* **2001**, *356*, 503–515.
(20) Loizou, E.; Butler, P.; Porcar, L.; Kesselman, E.; Talmon, Y.; Dundigalla, A.; Schmidt, G. *Macromolecules* **2005**, *38*, 2047–2049.
(21) Baghdadi, H. A.; Parrella, J.; Bhatia, S. R. *Rheol. Acta* **2008**, *47* (3), 349–357.
(22) Zulian, L.; Ruzicka, B.; Ruocco, G. *Philos. Mag.* **2008**, *88* (33−35), 4213–4221.
(23) Zebrowski, J.; Prasad, V.; Zhang, W.; Walker, L. M.; Weitz, D. A. *Colloids Surf., A* **2003**, *213*, 189–197.
(24) Pozzo, D. C.; Walker, L. M. *Colloids Surf., A* **2004**, *240*, 187–198.
(25) Otsubo, Y. *J. Rheol.* **1993**, *37* (5), 799–809.
(26) Loizou, E.; Porcar, L.; Schexnailder, P.; Schmidt, G.; Butler, P. *Macromolecules* **2010**, 43.
(27) Schmidt, G.; Nakatani, A. I.; Butler, P. D.; Karim, A.; Han, C. C. *Macromolecules* **2000**, *33*, 7219–7222.
(28) Schmidt, G.; Nakatani, A. I.; Butler, P. D.; Han, C. C. *Macromolecules* **2002**, *35*, 4725–4732.
(29) Matsunaga, T.; Endo, H.; Takeda, M.; Shibayama, M. *Macromolecules* **2010**, *43*, 5075–5082.
(30) Endo, H. *Physica B* **2006**, *385−386*, 682–684.
(31) Devanand, K.; Selser, J. C. *Macromolecules* **1991**, *24*, 5943–5947.
(32) Okabe, S.; Karino, T.; Nagao, M.; Watanabe, S.; Shibayama, M. *Nucl. Instrum. Methods Phys. Res., Sect. A* **2007**, *572*, 853–858.
(33) Takahashi, T.; Shirakashi, M.; Miyamoto, M.; Fuller, G. G. *Rheol. Acta* **2002**, *41*, 448–455.
(34) Kume, T.; Hashimoto, T.; Takahashi, T.; Fuller, G. G. *Macromolecules* **1997**, *30*, 7232–7236.
(35) Odtsubo, Y.; Umeya, K. *J. Rheol.* **1984**, *28*, 95–108.
(36) Shibayama, M.; Kawada, H.; Kume, T.; Sano, T.; Matsunaga, T.; Osaka, N.; Miyazaki, S.; Okabe, S.; Endo, H. *J. Chem. Phys.* **2007**, *127*, 144507.
(37) Prestrelski, S. J.; Bler, D. M.; Thompson, M. P. *Biochemistry* **1991**, *30*, 8798.
(38) Mourchid, A.; Levitz, P. *Phys. Rev. E* **1998**, *57*, R4887.
(39) Provencher, S. W.; Stepanek, P. *Part. Part. Syst. Charact.* **1996**, *13*, 291.
(40) Shibayama, M.; Norisuye, T. *Bull. Chem. Soc. Jpn.* **2002**, *75*, 641–659.
(41) Matsunaga, T.; Shibayama, M. *Phys. Rev. E, Rapid. Commun* **2007**, *76*, 030401.
(42) Shibayama, M.; Suda, J.; Karino, T.; Okabe, S.; Takehisa, T.; Haraguchi, K. *Macromolecules* **2004**, *37* (25), 9606–9612.
(43) Nishida, T.; Endo, H.; Osaka, N.; Li, H.-J.; Haraguchi, K.; Shibayama, M. *Phys. Rev. E* **2009**, *80*, 030801.
(44) Endo, H.; Schwahn, D.; Cölfen, J. *J. Chem. Phys.* **2004**, *120*, 9410–9423.
(45) Kawada, H.; Kume, T.; Matsunaga, T.; Iwai, H.; Sano, T.; Shibayama, M. *Langmuir* **2010**, *26*, 2430–2437.
(46) Endo, H.; Miyazaki, S.; Haraguchi, K.; Shibayama, M. *Macromolecules* **2008**, *41*, 5406–5411.